RSC Advances

ROYAL SOCIETY OF CHEMISTRY

www.rsc.org/advances

Reactive deposition of laser ablated FeS_{1-x} particles on copper surface.

J. Pola [a], M. Urbanová [a], D. Pokorná [a], P. Bezdička [b], J. Kupčík [b], T. Křenek [c]

[a] Laboratory of Laser Chemistry, Institute of Chemical Process Fundamentals of the ASCR, 16502 Prague, Czech Republic

[b] Institute of Inorganic Chemistry of the ASCR, 25068 Husinec-Řež, Czech Republic

[c] Research Centre of New Technologies, University of West Bohemia, 30614 Plzeň, Czech Republic

Abstract:

Pulsed IR laser ablation of ferrous sulfide (FeS) in a vacuum has been studied by using scanning and transmission electron microscopy and X-ray diffraction for the analysis of surface morphology and composition of the irradiated target and the coats deposited on unheated Ta, silica and Cu substrates. It is observed that a noncongruent ablation of FeS results in the deposition of nanosized FeS-containing FeS_{1-x} amorphous coats on silica and tantalum and in the deposition of crystalline copper sulfides-containing amorphous Cu_2S phase on copper. The detected amorphous Cu_2S phase and crystalline and nanocrystalline chalcocite Cu_2S, bornite Cu_5FeS_4, digenite Cu_9S_5 and blaubleibend covelite are formed through a reactive deposition of FeS_{1-x} particles on topmost Cu layers. This finding is the first example of reactive deposition of laser ablated inorganic compounds on unheated surfaces and may spur more interest in using this simple process with various inorganic compounds to achieve reactive modifications of other materials.

Keywords: ferrous sulfide, laser noncongruent ablation, amorphization, reactive deposition, copper sulfide films.

1. Introduction

Laser ablation has been broadly studied in the past 30 years (e.g.[1-5]) and became important in various fields of physics[1,2], chemistry[3] , medicine[4], material science[5] and mineral analysis[6,7]. The material removal induced by high-energy laser pulses, consisting in vaporization or ejection of excited neutral and/or charged fragments which agglomerate and condense at nearby substrate surface, has also proven a great potential for the deposition of smooth and nanostructured films and nanosized particles from elemental, inorganic and organic bulk materials (e.g.[8,9]). These deposits preserve or not the phase and the stoichiometry of bulk precursors depending on the ability of ejected particles to survive fast laser excitation and post-pulse cooling during deposition to substrate surface.

The purposeful laser ablative modification of morphology and structure of solid materials is achieved via laser ablation of mixed or dispersed elemental powders[10-14] and polymers (e.g.[15-17]) and by laser ablation of bulk elemental solids in the presence of a reactive gas (e.g. oxygen[18-21], nitrogen[22-24], carbon monoxide[25-27], hydrocarbon[28,29], or hydrogen sulfide[30]). All these processes are called *reactive laser ablation* and yield, in the given order, mixed clusters and nanosized products (e.g. intermetallics), structurally modified polymer particles and films, and binary, ternary or multielement (ceramic) compounds like oxides, nitrides, silicon or titanium oxycarbides, carbides and sulfides.

There are plenty of examples on reactive laser ablation for deposition of various materials with advanced properties. In these processes, materials with morphology or structure different from their bulk progenitors deposit due to high-temperature reactions taking place on the irradiated target and/or reactions of ejected fragments and agglomerates in the plume.

The structural or compositional modification of laser ablated particles through reactive collision with unheated substrate surface appears to have attracted little or no attention, although similar phenomenona - reactive deposition epitaxy (e.g.[31,32]) and deposition of multicomponent nanostructures (e.g.[33-38]) involving laser ablative deposition on *in-situ* or additionally heated substrates have been given much attention and is now part of high temperature solid–liquid state chemistry.

Thus, there is also missing information on the reactive deposition of laser ablated inorganic compounds on unheated surfaces, in spite that laser ablation of metal oxides, phosphides, chalcogenides and metal carbonyls was explored for the formation and interaction of inorganic cluster ions in the plume (e.g.[39-45]) and that laser ablation of mixed oxides[34,37], III-V compounds[46] and CdX (X=S,Se,Te)[35,37] powders was examined for the growth of nanostructures on furnace-heated substrates. The only reported data concern the laser ablative deposition of pyrite (FeS_2) and hematite (Fe_2O_3) on aluminium and silica and show that the deposited films at room and higher temperatures contain FeS and FeO constituents[47].

Herein we report on the pulsed IR laser ablative deposition of ferrous sulfide FeS on unheated silica, tantalum and copper substrates. The ferrous sulfide and its films are of interest due to their environmental reactivity, structural and phase-transition, and electrical and magnetic properties. We present SEM-EDX and XRD investigation of the FeS ablation and reveal that ablated iron sulfide particles form amorphous S-deficient coats on Ta and silica and that they react with unheated copper to produce copper sulfides. These results give support to further investigations of reactive depositions of laser ablated particles on various unheated substrates.

2. Experimental

The IR laser irradiation experiments were conducted in a vacuum (better than 10^{-3} Torr) in a previously described Pyrex reactor (70 mL in volume)[48] which consisted of a tube fitted at each end with NaCl windows and a valve connecting to vacuum manifold and pressure transducer. We used a pulsed TEA CO_2 laser (model 1300 M, Plovdiv University) operating with a frequency of 1 Hz on the P(20) line of the 00^01-10^00 transition (944.19 cm^{-1}), the full width at half maximum (FWHM) of 150 ns and a pulse energy of 1.4 J. The radiation was focused with a NaCl lens (f. l. 15 cm) on the FeS pellet positioned in the centre of the reactor above which were accommodated copper, tantalum and silica substrates in the distance 1 cm afar from the target. A simple irradiation scheme is given in Fig. 1. The effect of the distance of the Cu substrate on the morphology of the deposited coats was examined for the substrate-target distance 1 mm, 3 cm, 7 cm and 9 cm. The focus point was adjusted at the target to get incident energy fluence 140 $J.cm^{-2}$. After irradiation with 700 pulses, the reactor was opened to atmosphere and the substrates covered with the deposited coats were transferred for the measurements of coat properties by

electron microscopy and X-ray diffraction analysis. Electron microscopy studies were performed on a SEM Tescan Indusem (Bruker Quantax) microscope equipped with an EDAX detector and on a JEOL JEM 3010 TEM microscope.

Transmission electron microscopy (TEM) analysis (particle size and phase analysis) was carried out with a JEOL JEM 3010 microscope operating at 300 kV and equipped with an EDS detector (INCA/Oxford) and CCD Gatan (Digital Micrograph software) on scraped samples that were subsequently dispersed in ethanol followed by application of a drop of a diluted suspension on a polymer/carbon coated Cu grid. The diffraction patterns were evaluated using JCPDS-2 database[49] and Process Diffraction software package[50].

Diffraction patterns were collected with a PANalytical X´Pert PRO diffractometer equipped with a conventional X-ray tube (Co K_a radiation, 40 kV, 30 mA, point focus), an X-ray monocapillary with diameter of 0.1 mm, and a multichannel detector X'Celerator with an anti-scatter shield. A sample holder for single crystal XRD measurement was adopted by adding z-(vertical) axis adjustment (Huber 1005 goniometer head). We assumed that the layer produced was very thin, so we decided to fix the angle of the incident beam (omega) to 1.5 degree to suppress the penetration depth and to enhance the signal of the layer. The diffraction patterns were taken between 10 and 90° 2Θ with 0.0334° step and 2000 s counting time per step that produces total counting time of about 12 hours. XRD patterns were not pre-treated before interpretation as no background correction was-needed. Qualitative analysis was performed with HighScore software package (PANalytical, Netherlands, version 1.0d), Diffrac-Plus software package (Bruker AXS, Germany, version 8.0) and JCPDS PDF-2 database[49].

Raman and FTIR spectra were also measured, but they did not show any characteristic features. The FeS pellet was made at 100 atm. on a hydraulic press from a commercially available iron sulfide powder (FeS, 99% Fe, Aldrich).

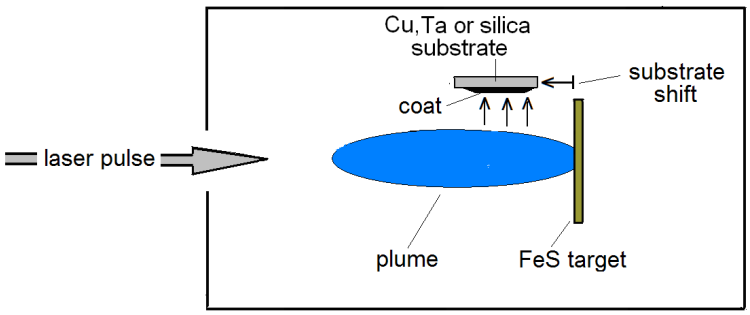

Fig. 1. Scheme of laser ablative deposition.

3. Results and discussion

The IR laser irradiation of the FeS pellet in the vacuum results in the pellet ablation and a visible luminescence (plasma) observed as a bluish ca. 1 cm wide and 7 cm long plume. Similar plumes of excited fragments during IR laser ablations were previously observed for the IR laser ablation of metals[51] due to transient formation of metal atoms and ions[52]. The ablation leads to the development of a crater and the deposition of ejected particles on adjacent Ta, silica and Cu substrates (Fig. 2), where they form layers of different appearance. The coats on Ta and silica are smooth, but those on copper are not homogeneous and show areas detached from the surface.

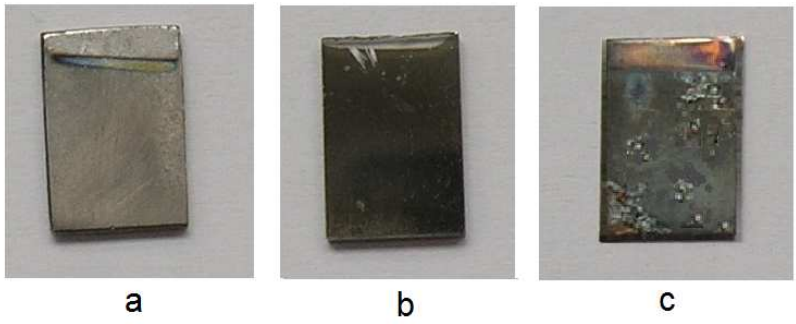

Fig. 2. The coated Ta (a), silica (b) and Cu (c) substrates.

The SEM images of the irradiated spot (Fig. 3) reveal melting, formation of column-like features pushed from a ca. 1 mm^2 sized crater, and ejection of several μm-sized objects and droplets that deposit on the crater periphery. The images of the coats deposited on silica and Ta show μm-sized round-shape objects in continuous surroundings (Fig. 4a,b), whereas those of the coat deposited on Cu show large flat peeled off bodies occurring near shapeless agglomerates (Fig. 4c). These features are in accordance with vaporized and plasma-produced clusters and liquid droplets expelled from the target surface and quenched upon deposition. The round-shaped objects on silica and Ta indicate rapid cooling of solidifying droplets which may occur in a metastable amorphous state. Furthermore, a high energy of these particles prior to collisions with the substrate surface is proved by splattering and trails. The flat entities extending from Cu surface and occurring together with irregular agglomerates and droplets indicate the formation of a new phase.

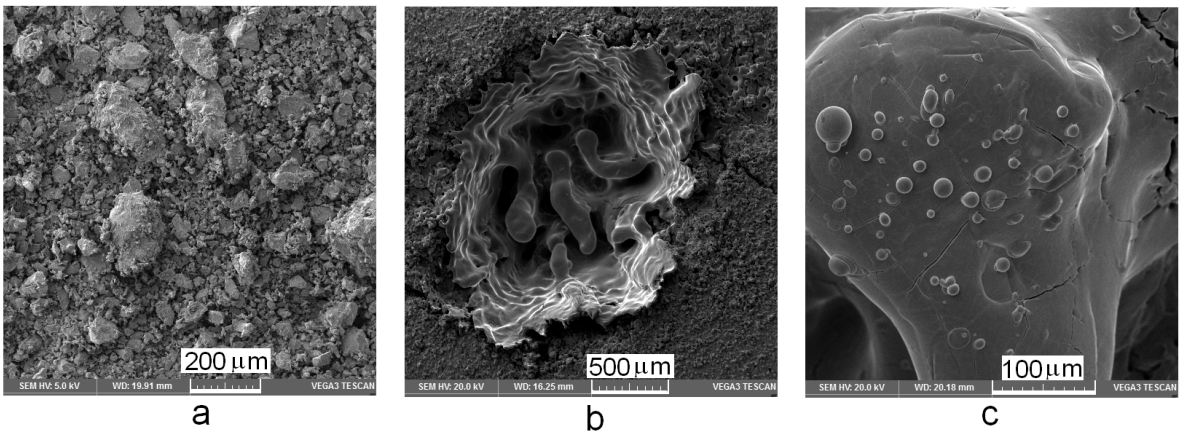

Fig. 3. SEM images of the FeS powder (a) the irradiated spot (b) and the crater periphery (c).

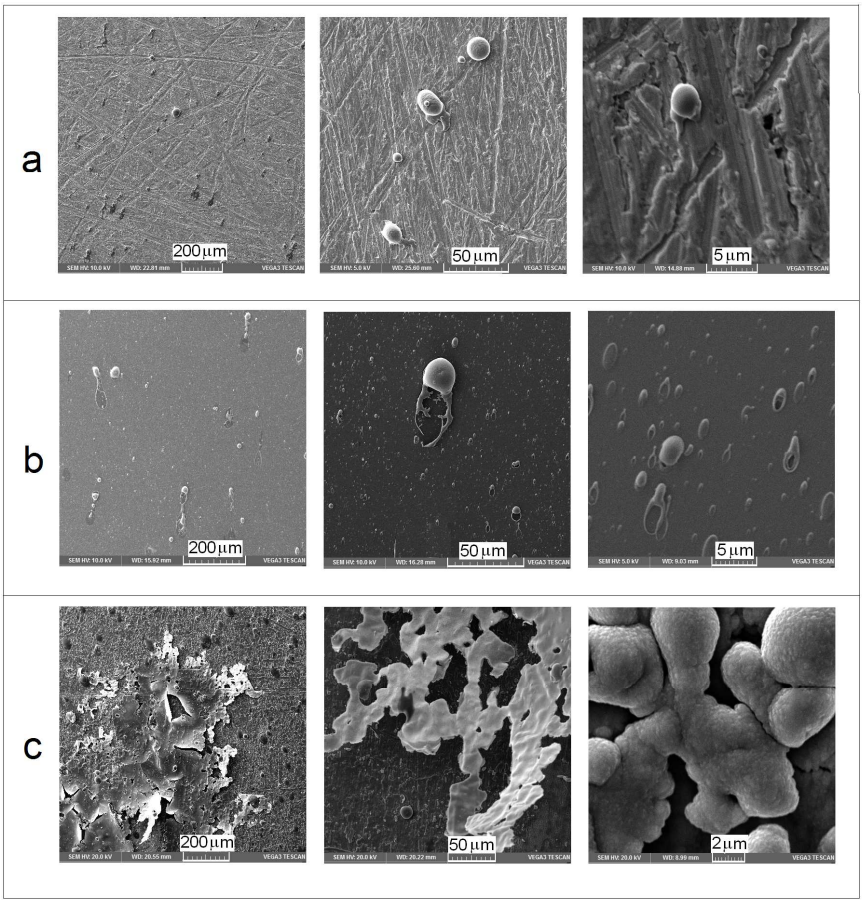

Fig. 4. SEM images of coats deposited on Ta (a), silica (b) and Cu (c) substrates.

The EDX-SEM analyses allow assess the composition of the coats and have been performed on the crater and its periphery, the μm-sized particles near the crater and the deposited coats (droplets, agglomerates and smooth areas, Table 1). The S/Fe atomic percent ratios of the crater and its periphery (0.85 ± 0.02) and the droplets near the crater (0.74 ± 0.06) are somewhat lower than those of the initial FeS sample (0.94 ± 0.02). These values indicate some decomposition of FeS. Such incongruent deposition of S-deficient coats is also observed on Ta and silica, where the μm-sized droplets have the S/Fe ratios even lower than those near the crater and where smooth areas have more S than Fe, which is assignable to a fast diffusion of Fe to lower Ta and SiO_2 layers.

Regarding the coats on Cu, the S/Fe and Cu/Fe atomic percent ratios for the flat bodies and the proximal shapeless areas reflect similar Cu/S ratios and highly diminished Fe contents in both features. There are very few several-μm sized isolated droplets on Cu surface which have S/Fe ratio 0.64 and which correspond to the particles seen on Ta and silica. We assume that the flat and shapeless areas were produced by collisions of both FeS_{1-x} clusters and μm-sized FeS_{1-x} particles with Cu surface, and that their different appearance arises from charge- or energy-inhomogeneous flow of colliding FeS_{1-x} species.

Table 1. EDX-SEM analysis[a] of coats deposited on Ta, silica and Cu.

Object /substrate	Ta	SiO_2	Cu	
	S/Fe	S/Fe	S/Fe	Cu/Fe
μm-sized droplets	0.75 ± 0.07	0.50	0.64 ± 0.03	0 - 0.2
smooth area	2.0 ± 0,50	1.35 ± 0.05	-	
flat bodies	-	-	23-32	54-58
shapeless area	-	-	8.0 - 14.4	14,7- 27,0

[a]S/Fe/ and Cu/Fe atomic percent ratios.

It is known that plasma vapor and liquid droplets move at high speed and that their flight distance and cooling rate after impact to surface diminish with their mass. The SEM images (Fig. 5) and the EDX analysis of the deposited areas for different distances between the Cu substrate and the target reveal a substantial deposition for areas 1mm and 3 cm afar from the target, a low

deposition for the distance of 7 cm and no deposition for the distance of 9 cm (not shown). The large several μm-sized flattened bodies and the droplets with S/Fe atomic percent ratio 0.67 occur near the target together with coated area having the S/Fe values 3.5 and the Cu/Fe values 98. These features respectively correspond to incongruent FeS particles and reactive deposition of smaller particles on copper. The flat and amorphous features without large droplets are seen at the distance of 3 cm from the target and they consist of Cu and S (Cu/S = 5.1-5.4) and a very low amount of Fe (ca 0.1 percent of S). These large plates and the agglomerates have the same composition and are also in line with reactive deposition. Farther areas at the 7 cm distance show no Fe and their Cu/S ratio 24-25 indicates a thin layer with a prevalence of Cu substrate.

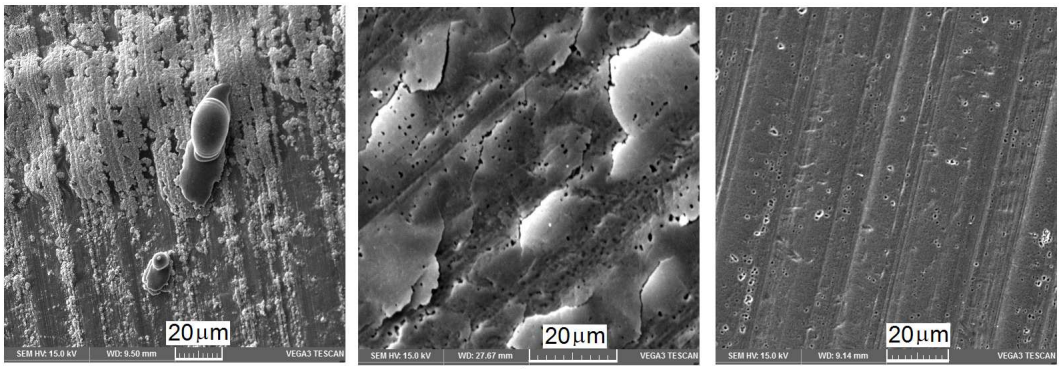

Fig. 5. SEM images of coat on Cu substrate 1 mm (a), 3 cm (b) and 7 cm (c) afar from target.

The X-ray diffraction analysis of the commercial FeS sample allows the estimation of relative amounts crystalline troilite (~ 63%), pyrrhotite (~ 24%) and alpha-Fe 13%. The XRD analysis of the coat deposited on Ta shows only FeS (troilite) and no diffraction lines on silica, the latter being consistent with an amorphous phase. The analysis of the coat deposited on Cu reveals the presence of two Cu-containing sulfides, specifically digenite and bornite (Fig. 6).

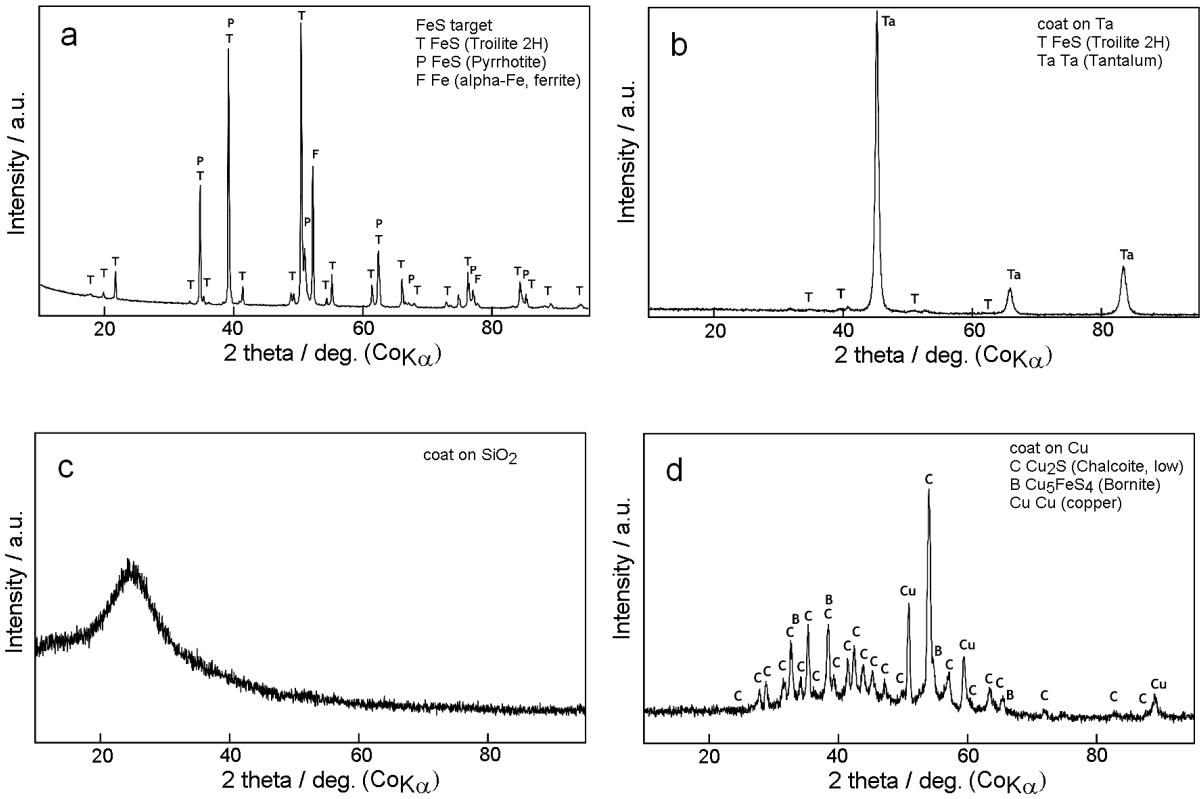

Fig. 6. XRD pattern of FeS target (a) and coats deposited on Ta (b), silica (c) and Cu (d) substrates.

The TEM and ED examinations of the coats on Ta, silica and Cu reveal a number of areas with both discrete diffraction lines and halo patterns, which are in line with the occurrence of nanocrystalline and nanoamorpous regions. These analyses (Fig. 7) indicate ca. 2 nm-sized hexagonal FeS nanograins on Ta and silica and show that the nanograins on silica escaped their identification by XRD analysis. There are more distinct FeS diffraction rings on silica than on Ta, which is in line with less amorphization of nanograins on silica due to slower cooling of solidifing fragments on the low thermal conductivity substrate.

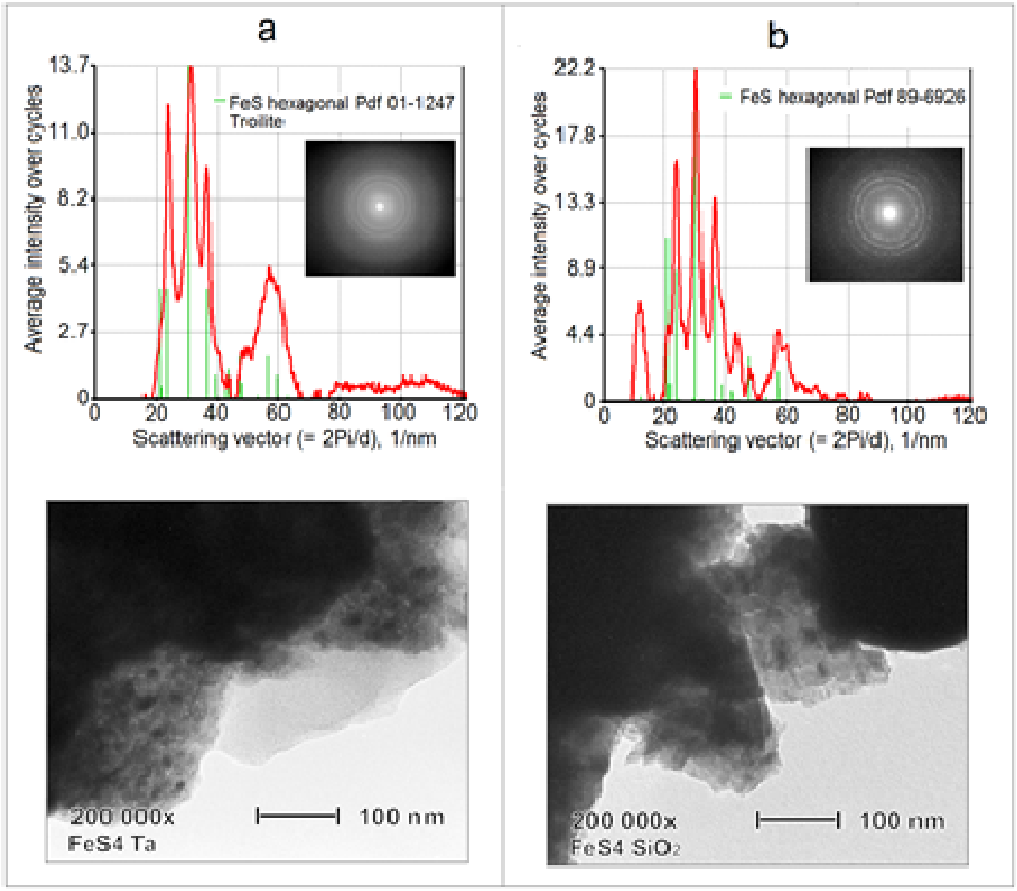

Fig. 7. TEM and electron diffraction images of coats on Ta (a) and silica (b).

The examination of the coats on Cu shows the occurrence of amorphous and crystalline nanophases. The observed single crystal diffraction patterns as well as polycrystalline ring diffraction patterns are respectively consistent with ca. μm-sized objects and polycrystals composed of nm- sized grains. Both were found in peeled off plates and shapeless bodies (Fig. 8). The ED analysis is consistent with the occurrence of chalcocite, digenite, bornite and blaubleibend covelite.

We note that the absence of any characteristic features in the IR and Raman spectra of the coats on Cu can be therefore ascribed to the fact that the copper sulfides are poorer IR absorbers and also weaker Raman scatters, not mentioning that the symmetrical Cu_2S is not amenable to internal dipole changes required for Raman analysis.

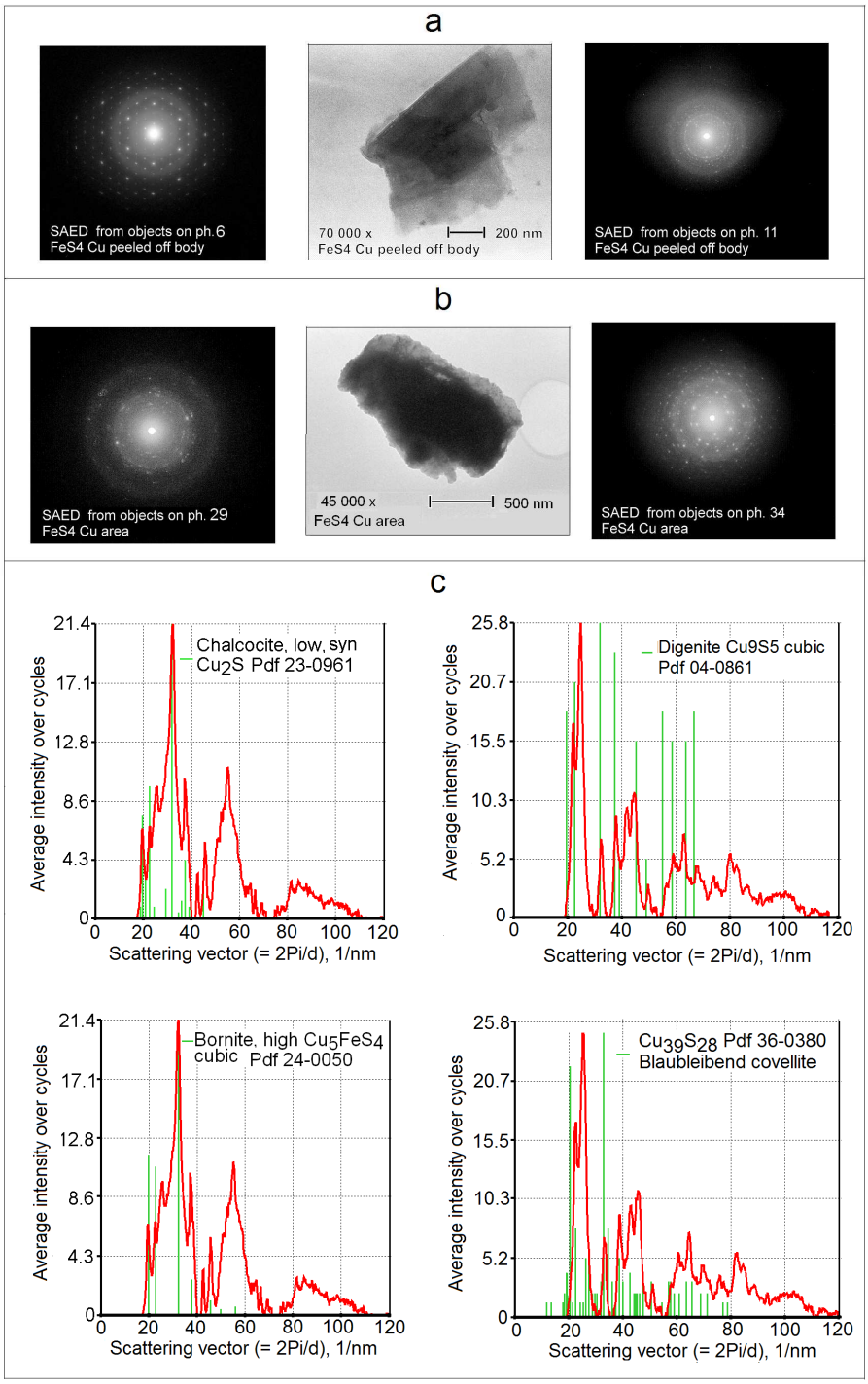

Fig. 8. TEM and electron diffraction images of coats on Cu: a and b respectively relate to peeled off plates and irregular surface-attached agglomerates; (c) shows ED images found on both regions.

These complementary analyses are therefore in line with the deposition of FeS nanograins-containing amorphous FeS_{1-x} phase on Ta and silica and with the reactive deposition of μm- and several nm-sized crystalline sulfides and amorphous copper sulfides on Cu. The morphpological inhomogeneity of the Cu coats, manifesting itself as shapeless and flat-bodies areas, is apparently due to reactive colllisions of FeS_{1-x} particles and clusters which differ in mass, energy and charge[13,14,41]. We suggest that high-energy interactions of colliding FeS_{1-x} particles and clusters are a driving force for FeS_{1-x} - Cu interdiffusion and crystalline sulfidic phase formation, while interactions of less energetic particles can be sufficient only for the formation of amorphous phase.

The mechanism of the massive formation of copper sulfidic phase can be discussed in relation to some previous findings on metal exchange and formation of these entities in other systems. It is known that heavy metal (M) ions react with insoluble FeS in aqueous solution via $FeS + M^{2+} \rightarrow MS + Fe^{2+}$ reaction[53] and that discrete particles of copper sulphide $Cu_{1.8}S$ (digenite) are precipitated from the high temperature oxidizing environment during welding of sulfur-bearing steels in the presence of soluble copper, which is thought to be due to a reaction between copper and less stable ferrous sulphide present in these steels ($2\ FeS + 4Cu + O_2 \rightarrow 2\ Cu_2S + 2\ FeO$)[54]. Our findings of copper sulfides formation in the absence of air is consistent with metal-metal sulfide exchange through reduction of Fe^{II} and oxidation of Cu^0, which is likely enhanced by both high energy and charge-bearing FeS_{1-x} clusters diffusing into the copper surface.

The presented results have three implications. First, the stoichiometric FeS, occuring as troilite and the less stable amorphous phase, experiences phase transitions upon annealing prior to its decomposition at 1260 K[55], even though a partial decomposition to $FeS_{0.91}$ begins at above 500 ^oC[56]. The observed IR laser ablation leading to the FeS_{1-x} coats may be optimized for fabrication of more homogeneous films of various compositions and also for films structurally similar to mackinawite whose properties, contrary to those of pyrrhotite ($Fe_{1-x}S$)-type films and nanostructures[57], have not been yet studied. In this regard, the use of other irradiation wavelengths and pulse durations emitted by other (excimer, near IR, or pico-and femtosecond) lasers procuring conditions for more photochemical than thermochemical action may be highly hopeful.

Second, copper sulfides are usually obtained by solid-state reactions of elements, metathesis or self-propagating high-temperature synthesis. Digenite (Cu_9S_5) occurring as the high-, the

metastable- and the-low- polymorph is usually prepared by melting method, in solution, or by mechanical alloying. The low-digenite is stable at room temperature only, if it contains a small amount of Fe, while the high digenite, isostructural with bornite (Cu_5FeS_4), is stable[58-60] only at above 73 ^oC. These materials may decompose to binary alloys which can become promising thermoelectric materials like e.g. Cu_9S_5 decomposing[61] to $Cu_{1.96}S$. Further optimization of the formation of copper sulfides and other metal sulfides by using reactive laser deposition at various laser wavelengths and fluences is therefore worth examining.

Third, the bornite and digenite formation upon fast quenching during the reactive deposition of FeS_{1-x} particles illustrates that the process of the reactive laser deposition may help to understand formation of intermediary compositions in the course of important thermodynamically equilibrium geological processes like exsolution of metal sulfides[62] and other natural ore assemblages. The technique of laser ablative deposition of mineral ores or synthesized model samples may serve for this purpose.

Our results encourage more investigations of reactive deposition of laser ablated particles rapidly quenched on unheated substrates, especially on materials which are unstable at higher temperatures and can offer specific reactivity towards energized ablated particles at room temperature. More work on a possible use of the technique for examination of such solid-state chemistry is in progress.

4. Conclusion

The pulsed IR laser ablation of ferrous sulfide (FeS) results in the deposition of FeS nanocrystals-containing amorphous sulfur-poorer FeS_{1-x} coats on silica and tantalum, and the deposition of nanocrystalline copper sulfides (chalcocite Cu_2S, bornite Cu_5FeS_4, digenite Cu_9S_5 and blaubleibend covelite)-containing amorphous Cu_2S phase on copper.

These coats are formed by somewhat noncongruent FeS ablation and amorphization of high-energy particles which rapidly cool upon collisions with the ambient-temperature substrates.

The coats on Cu result from reaction(s) between high-energy FeS_{1-x} particles and copper surface and their morphpological inhomogeneity obviously reflects collisions of particles differing in energy and size.

The results encourage further exploration of the reactive laser deposition of ablated inorganic compounds on unheated surfaces due to potential of this technique for synthesis of inorganic films and recognition of rapidly quenched intermediate stages during exsolution of minerals.

Acknowledgements: The research was carried out within the CENTEM project, reg. no. CZ.1.05/2.1.00/03.0088, co-funded by the ERDF as part of the Ministry of Education, Youth and Sports' OP RDI programme.

References

1. Laser ablation, Principles and applications, J.C. Miller, ed., Springer-Verlag, Berlin, 1994.
2. Laser Ablation and its Applications, C. Phipps, ed., Springer Series in Optical Science vol. 129, Springer, New York, 2007.
3. Laser ablation of molecular structures, S. Georgiou, A. Koubenakis, guest eds. *Chem. Rev*. 2003, **103**, issue 2.
4. T.F. Deutsch, IR-laser ablation in medicine: Mechanisms and applications. *Lecture Notes in Physics* 1991, **389**, 107-111.
5. D. Bäuerle, Laser Processing and Chemistry, Springer-Verlag, Berlin, Heidelberg, 2000.
6. A.J. Campbell, M. Humayun, *Anal. Chem*. 1999, **71**, 939-946.
7. B. Yan, L. Li, Q. Yu, W. Hang, J. He, B. Juany, *J. Am. Soc. Mass Spectrom*. 2010, **21**, 1227–1234 and refs. therein.
8. Pulsed Laser Deposition of Thin Films D.B. Chrisey, G.K. Hubler, eds., Wiley-Interscience, New York, 1994.
9. Laser ablation, E. Fogarassy, D. Geohegan, M. Stuke, eds., MRS Symp. Proc. 55, Elsevier, Amsterdam, 1995.
10. X. Zhang, G. Li, Z. Gao, *Rapid Commun. Mass Spectrom*. 2001, **15**, 1573-1576.
11. J. K. Gibbon, J. Vac. Sci. Technol. A, 1997, **15**, 2107-2118.
12. G. Glaspell, V. Abdelsayed, K. M. Soud, M. S. El-Shall, *Pure Appl. Chem.* 2007, **78**, 1667–1689.

13. J.-B. Liu, C.-Y. Han, W.-J. Zheng, Z. Gao, Q.-H. Zhu, *Int. J. Mass Spectrom*. 1999. **189**, 147–156.

14. J. Houska, M. Alberti, J. Havel, Rapid Commun. Mass Spectrom. 2008, **22**, 417–423.

15. T. Lippert, UV Laser Ablation of Polymers: From Structuring to Thin Film Deposition, in Laser-Surface Interactions for New Materials Production, Springer Series in Materials Science, 130, 141-175 (2010).

16. J. Pola, J. Kupčik, S. M. A. Durani, E. E. Khavaja, H. M. Masoudi, Z. Bastl, J. Šubrt, 2003, *Chem. Mater.* 2003, **15**, 3887–3893**.**

17. J. Pola, J. Kupčík, V. Blechta, A. Galíková, A.Galík, J. Šubrt, J. Kurjata, J. Chojnowski, *Chem. Mater*. 2002, **14**, 1242–1248**.**

18. G. P. ReaJohnston, R. Muenchausen, D. M. Smith, W. Fahrenholtz, S. Foltyn, *J. Am. Ceram. Soc*. 1992, **75**, 3293–3298.

19. R. Castro-Rodríguez, A. Iribarren, P. Bartolo-Pérez, J.L. Peña, *Thin Solid Films* 2005, **484**, 100-103.

20. C.-N. Huang, S.-Y. Chen, M.-H. Tsai, P. Shen, *J. Cryst. Growth* 2007, **305**, 285–295.

21. T. Yoshida, H. Toyoyama, I. Umezu, A. Sugimura, *Appl. Phys* A. 2008, **93**, 961-966.

22. X.-A Zhao, C.W. Ong, Y. C. Tsang, Y.W. Wong, P. W. Chan, C.-L. Choy, *Appl. Phys. Lett*. 1995, **66**, 2652-2654.

23. G. Soto, J.A. Díaz, W. de la Cruz, *Mater. Lett*. 2003, **57**, 4130-4133.

24. G. Soto, J. A. Diaz, R. Machorro, A. Reyes-Serrato, W. de la Cruz, *Mater. Lett*. 2002, **52**, 29–33.

25. M. Urbanová, D. Pokorná , S. Bakardjieva, J. Šubrt, Z. Bastl , J. Pola, *Eur. J. Inorg. Chem*. 2008, 4111-4116.

26. V. Jandová, J. Kupčík, Z. Bastl , J. Šubrt, J. Pola, *Solid State Sci*. 2013, **19**, 104-110.

27. J. Pola, S. Bakardjieva, M. Maryško, V. Vorlíček, J. Šubrt, Z. Bastl, A. Galíková, A. Ouchi, *J. Phys. Chem.* C 2007, **111**, 16818-16826.

28. G. Leggieri, A. Luches, M. Martino, A. Perrone, G. Majni, P. Mengucci, I.N. Mihailescu, *Thin Solid Films* 1995, **258**, 40-45.

29. J. Pola, M. Urbanová, D. Pokorná, J. Šubrt, S. Bakardjieva, P. Bezdička, Z. Bastl, *J. Photochem. Photobiol.* A 2010, **210**, 153-161.

30. G.D. Surgina, A.V. Zenkevich, I.P. Sipaylo, V.N. Nevolin, W. Drube, P.E. Teterin, M.N. Minnekaev, *Thin Solid Films*, 2013, **535**, 44-47.

31. H. Zhou, G. Henn, M. Gross , H. Schröder, F. Phillipp, *Phys. stat. sol.* (a) 2001, **188**, 1065–1070.

32. H. Ohta, *J. Ceram. Soc Jap*. 2006, **114**, 147-154.

33.J. Hu, T. W. Odom, C. M. Lieber, *Acc. Chem. Res*. 1999, **32**, 435-445.

34. Y.F. Zhang, Y.H. Tang, X.F. Duan, Y. Zhang, C.S. Lee, N. Wang, I. Bello, S.T. Lee, *Chem. Phys. Lett*. 2000, **323**, 180–184.

35. Y.-J. Choi, I.-S. Hwang, J.-H. Park, S.Nahm, J.-G. Park, *Nanotechnology* 2006, **17**, 3775–3778.

36. S. Neretina, P. Mascher, R.A. Hughes, N. Braidy, W.H. Gong, J.F. Britten, J.S. Presto, N.V. Sochinskii, P. Dippo, *Appl. Phys. Lett*. 2006, **89**, 133101- 3 pp.

37. R. Savu, E. Joanni, *Scripta Mater.* 2006, **55**, 979–981.

38. K. Namiki, D. Yokoyama, Y. Yamada, *AIP Conf. Proc.* 2005, **765**, 114-119.

39. I.G. Dance, K.J. Fisher, G.D. Willett, *J. Chem. Soc., Dalton Trans*., 1997, 2557-2562.

40. F. Aubriet, C. Poleunis, J.-F. Miller, P. Bertrand, *J. Mass Spectrom*. 2006, **41**, 527–542.

41. J.H. El Nakat, I. G. Dance, K. J. Fisher, D. Rice, G.D. Willettt, *J. Am. Chem. Soc*. 1991, **113**, 5141-5148.

42. F. Aubriet, J.-F. Miller, *J. Am. Soc. Mass Spectrom*. 2008, **19**, 488–501.

43. A.V. Bulgakov, A.B. Evtushenko, Y.G. Shukhov, I. Ozerov, W. Marine, *AIP Conf. Proc*. 2010, **1278**, 78-89.

44. J.S. McIndoe, *Transit. Metal Chem*. 2003, **28**, 122–131.

45. J.-B. Liu, C.-Y. Han, W.-J. Zheng, Z. Gao, Q.-H. Zhu, *Int. J. Mass Spectrom*. 1999, **189**, 147–156.

46. W. Shi, Y.Zheng, N. Wang, C.-S. Lee, S.-T. Lee, *Adv. Mater*. 2001, **13**, 591-593.

47. D. Yokoyama, K. Namiki, Y. Yamada, *J. Radioanal. Nucl. Chem*. 2006, **268**, 283–288.

48. J. Pola, D. Pokorná, M. Maryško, Z. Bastl, J. Šubrt, S. Bakardjieva, P. Bezdička, M.A. Gondal, H.M. Masoudi, *J. Photochem. Photobiol*. *A: Chem*. 2011, **223**, 132-139.

49. JCPDS PDF-2 database, International Centre for Diffraction Data, Newtown Square, PA, U.S.A. release 54, 2004.

50. J.L. Lábár, M. Adamik, *Microscopy and Microanalysis* 2001, **7**, Suppl. 2, 372-373.

51. M. Urbanová, D. Pokorná, J. Šubrt, J. Kupčík, Z. Bastl, J. Pola, *J. Adv. Microsc. Res*. 2012, **7**, 14-20.

52. M. Santos, L. Díaz, J.J. Camacho, M. Urbanová, D. Pokorná, J. Šubrt, S. Bakardjieva, Z. Bastl, J. Pola, *Infrared Phys. Technol.* 2010, **53**, 23-28.

53. A.P. Davis, O.J. Hao, J.M. Chen, *Chemosphere* 1994, **28**, 1147-1164 and refs. therein.

54. J.E. Harbottle, S.B. Fisher, *Nature* 1982, **299**, 139 - 140.

55. H.E. King, C.T. Prewitt, *Acta Cryst.* B 1982, **38**, 1877-1887 and refs. therein.

56. J. Yan, L. Xu, J. Yang, *J. Anal. Appl. Pyrol*. 2008, **82**, 229-234.

57. M. Akhtar, A.L. Abdelhady, M.A. Malik, P. O´Brien, *J. Cryst. Growth* 2012, **346**, 106-112 and refs. therein.

58. N. Morimoto, G. Kullerud, *Amer. Mineral*. 1963, **48**, 110-123.

59. N. Morimoto, A. Gyobu, *Amer. Mineral.* 1971, **56**, 1889-1909.

60. G. Will, E. Hinze, A.R.M. Abdelrahman, *Eur. J. Mineral*. 2002, **14**, 591-598.

61. Z.-H. Ge, B.-P. Zhang, Y.-X. Chen, Z.-X. Yu, Y. Liu, J-F. Li, *Chem. Commun*. 2011, **47**, 12697-12699.

62. B.A. Grgurich, A. Putnis, *Mineralog. Magaz*. 1999, 63, 1-12.

Table of contents entry

Reactive deposition of laser ablated FeS_{1-x} particles on room-temperature copper surface allows formation of Cu sulfides